Friction limit prediction of high-strength bolted connections using finite element method

Mojtaba Hosseini, Amir Mohammad Amiri, Peyman Beiranvand, Esfandiyar Abasi

To cite this article

Disclaimer

Research Article

Friction limit prediction of high-strength bolted connections using finite element method

Mojtaba Hosseini[a], Amir Mohammad Amiri[b], Peyman Beiranvand[c], Esfandiyar Abasi [d]

Department of Civil Engineering, Lorestan University, Khorramabad, Iran

Article Info	Abstract
	In this study, the aim is to deduce the static friction limit of contact interfaces in bolt friction joints by analyzing other bolt friction joints with the same contact surface but in a different shape. By using the Weibull mathematical distribution to deal with microelements on the contact surface, the friction limit of a certain type of bolt connection was statistically predicted from other types of bolt connections with the same contact surface. As a result, this research succeeded to predict the friction limit of bolt joints with different numbers of contact surfaces and with different numbers of bolt rows. Another result of this research both the stress ratio and the Weibull stress ratio showed a high prediction accuracy.

1. Introduction

High-strength bolted friction (HSF) joints are widely used as field joints for structural members of steel bridges. HSF joints have many advantages such as easy construction, good rigidity, and good fatigue resistance. HSF joints have become one of the main connection types in steel bridges. Although three different Chinese specifications [1–3] and other specifications in the world [4,5] have specified design concepts of HSF joints, there still exist many issues remaining to be solved: such as the detailed stress state of the connected plate, the load transfer factor of each bolt, and the friction stress distribution of the contact surfaces. The bolt friction joints are widely used in steel structures. The friction coefficient is often used to evaluate the loading capacity of bolt friction joints and it is only decided by the contact surface specification like 0.45 for an organized zinc-rich paint surface (IOZ) and 0.4 for the blasted surface in design. However, experimentally obtained friction coefficients μ have dispersion even if they have been made by the same contact surface specification. It could be considered that the micro surface condition is ununiformed for many reasons, for example, the spatial dispersion in one surface [6], the number of contact surfaces [7], bolt columns [8], and so on. Experimental results showed that the friction coefficient of a double-lap bolt joint is slightly higher than that of a single-lap bolt joint both in IOZ and blasted surface [7], and friction coefficients also varied when the number of bolt columns changed [8].

Based on these issues, not only the contact surface specification but also many other reasons should also be considered in a real situation so that we can get a rational friction limit considering relationships between local stress and dispersion of micro surface condition. To achieve that, the computational simulation could be considered because it

provides detailed local stresses in contact surfaces and may efficiently save experimental costs at the same time.

Recently, the finite element (FE) method was used to investigate the behavior of this type of connection. Citipitioglu et al. [9] studied the influence of bolt pretension and the effect of friction and friction between the connection components on the behavior of such connections by using the FE method. In their FE models, all connection components were modeled using brick elements, while the effect of adjacent surfaces was considered. A FE model with 3-Dsolid elements was established to investigate the bearing failure of cold-formed steel bolted connections under shear by Chung a dip [10]. Ju et al. [11] used the 3-D elastoplastic FE method to study the structural behavior of the butt-type steel bolted joint. The numerical results were compared with AISC specification data.

Soo et al. [12] used the ABAQUS program to establish FE models with 3-D solid elements. Non-linear material and non-geometric analyses were carried out to predict the load-displacement curves of bolted connections. Su et al. [13] developed an iterative procedure through a computer program to calculate the non-linear deformation of bolt groups under in-plane eccentric loads based on the assumptions of elastoplastic behavior of bolts and rigid body movement of the bolt group. Yu et al. [14] explored the use of an explicit dynamic solver to analyze bolted steel connections. By comparing the results with those from static analysis and tests, it was shown that the explicit dynamic solver, with proper control, gives satisfactory predictions of the responses of steel connections up to post-failure deformations. Bouchair et al. [15] studied the behavior of stainless steel bolted connections.

This research focuses on the friction coefficients of different kinds of bolted joints with the same contact surface specification. This research aims to find a local approach-based rational method to predict the friction limit of many types of different high-strength bolt joints from experimentally obtained friction coefficients of one type of joint with the same contact surface specification. This research firstly speculates the friction limit of single-lap bolt joints from double-lap bolt joints and secondly speculates the friction limit of multi-rows bolt joints from 2-rows bolt joints.

2. Method and Materials

2.1. Subject Description

Fig. 1 shows the geometry of experimental specimens, and Table 1 shows their specifications. P2-15 and B2-10 (PB) are 2face friction joints, the former with inorganic zinc and the latter with blasted specimens. P1-15 and B1-10 (PB) are 1-face friction joints, the former with inorganic zinc and the latter with blasted specimens [7]. A structural steel SM490Y was used for the base plate and a connecting plate of the specimens, and F10T high-strength bolts (nominal diameter M22, length beneath the head 90 mm) were used. For the sliding side, a higher bolt axial force was introduced so that the main friction would precede on the friction side where the bolt axial force was controlled.

Rows of friction joints with blasted contact surfaces. SS41 was used for the base plate and connecting plates of the specimens, and F10T high-strength bolts (nominal diameter M20, length beneath the head 85 mm) were used and tightened to standard bolt tension (nominal value 18.2 t) on the sliding side [8]. If the ratio of friction/yield strength is smaller than 1 means bolt joints will have friction before baseboard yield when designed.
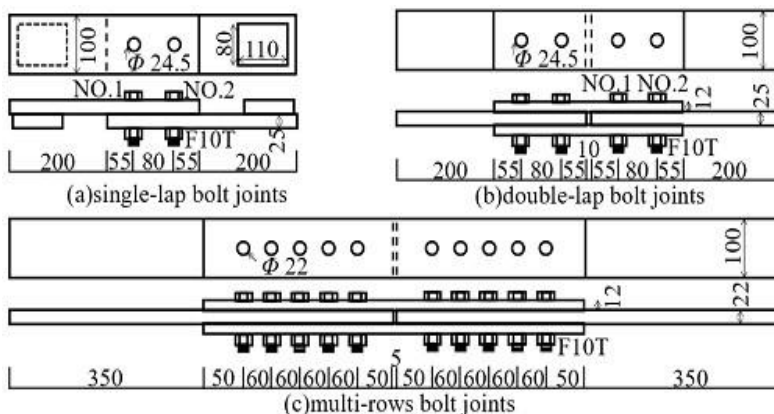
Fig. 1 Experimental specimens

Table 1. Specifications of experimental specimens

Specimens name	Contact surface	Number of contact surfaces	Rows of bolts	The ratio of friction/yield strength	Number of specimens
P1-15	IOZ	1	2	0.31	3
P2-15	IOZ	2	2	0.61	3
B1-10	Blast	1	2	0.24	3
B2-10	Blast	2	2	0.49	3
MB-20-2-12	Blast	2	2	0.8	2
MB-20-3-12	Blast	2	3	1.2	2
MB-20-4-12	Blast	2	4	1.6	2
MB-20-5-12	Blast	2	5	2.0	2

2.2. Experimental Methods and Results

In the friction capacity experiment of specimen PB, the bolt axial force was measured by strain gauges attached to the bolt shaft on the friction side immediately before loading, and the average strain on the front and back of the base plate was measured by strain gauges attached to the front and back of the base plate during the test, the amount of friction was measured by a clip gauge attached to the first bolt position on the friction side, and the load was measured by the load cell of the testing machine. A tensile load was applied at a loading rate of approximately 2kN/s until the main friction occurred.

In the friction capacity experiment of specimens MB, a 100-ton universal testing machine was used to apply a monotonic tensile force to the specimens. The average elongation of the joints of the specimens and the axial force of each bolt were measured with a strain gauge during the force application. Strain gauges were also attached to the shaft of the base plate, the base plate of the first bolt, and the connecting plate of the n-th bolt to measure the axial strain.

The results of the friction capacity test are shown in Table 2. In the PB experiment, his bolt axial force immediately before the test decreased significantly with time of more than one month after bolting. The coefficient of friction tended to be higher for the blasted specimens, and both the IOZ and blasted specimens showed a slightly higher coefficient of

friction for the specimens with single-lap bolt joints. The bending strain (the difference in strain between the front and back of the base plate divided by two) at the onset of main friction (when the friction capacity is reached) was about 1000μ for the specimens with single-lap bolt joints. In the MB experiment, the axial force variation during the experiment was measured with strain gauges at the bolt heads.

Table 2. The results of the friction capacity test

Specimens name		No.1 Bolt Load [kN]	No.2 Bolt Load [kN]	Average Bolt Load [kN]	Friction resistance [kN]	μ	Average μ
P1-15	-1	223	233	228.0	256	0.561	0.543
	-2	230	215	222.5	236	0.530	
	-3	217	231	224.0	241	0.538	
P2-15	-1	219	213	216.0	460	0.532	0.516
	-2	212	208	210.0	430	0.512	
	-3	221	226	223.5	450	0.503	
B1-10	-1	221	220	220.5	314	0.712	0.658
	-2	230	223	226.5	271	0.598	
	-3	229	225	227.0	302	0.665	
B2-10	-1	229	220	224.5	574	0.639	0.602
	-2	226	220	223.0	521	0.584	
	-3	227	215	221.0	516	0.584	
MB-20- 2-12	-1			181.6	521	0.718	0.670
	-2			181.2	451	0.622	
MB-20- 3-12	-1			184.1	570	0.516	0.518
	-2			185.0	576	0.519	
MB-20- 4-12	-1			183.8	635	0.432	0.431
	-2			179.8	620	0.431	
MB-20- 5-12	-1			181.3	658	0.366	0.368
	-2			182.2	674	0.370	

2.3. Analysis Conditions

The model that reproduces the behavior of each test piece up to the occurrence of main friction was created and used a high Static friction coefficient to fix friction displacement of the joint contact surface (using commercial software ABAQUS 2020).

Fig.2 shows an analytical model that reproduces the 1/2 region of the PB specimen and the 1/8 region of the MB specimen, in consideration of symmetry. Reduced integral first-order solid elements were used throughout. The contact surfaces were reproduced as flat surfaces with no surface roughness or coating. For the PB specimen model, the elements were divided to the thickness of 5mm for the base and connecting plate, and the circumference of the bolt holes was divided into small sections with a length of 3.5 mm. For the MB specimen, it was 4mm for thickness and 2.5mm for the area near bolt holes. Fig.3 shows the element partitioning around the bolt holes in multi rows bolt joints as an example test model. In the contact analysis, the base plate, connecting plate, and fasteners

(bolts, nuts, and washers integrated) were mobilized as independent elastic bodies with uniform material properties (Young's modulus 200GPa, Poisson's ratio 0.3), and contact conditions were applied to the interface between the base plate and connecting plate (contact surface of the joint) and between the connecting plate and the washer portion.

The static friction coefficients for the PB and MB joints surfaces were set to 20 and 30 percent respectively. This is determined by the specific situation of each specimen, to make the coefficient of friction of each element less than the set value at the moment of sliding, which means no relative sliding will occur. Using a higher coefficient of static friction, a similar solution will be obtained, but it will be more difficult to obtain the convergence solution.
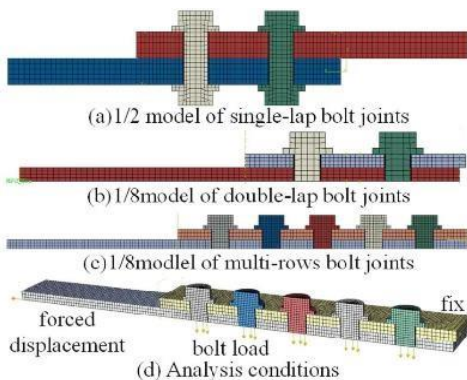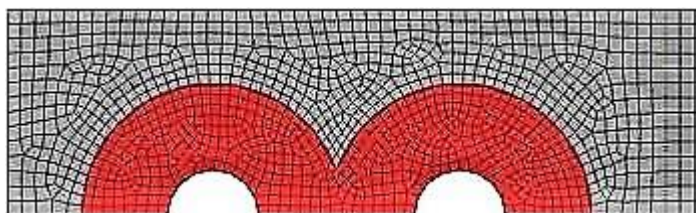

Fig. 2 Analysis models

Fig. 3 Mesh near the bolt holes

The contact determination is based on the penalty and extended Lagrange methods. Local friction is determined by the maximum frictional shear stress, which is determined by the contact pressure and the static friction coefficient.

The displacement was fixed at the end of the fixed base plate and the initial axial force during the test based on Table 2 was imposed at the bolt axial part by ABAQUS bolt load. The loading was then reproduced by applying a joint axial tension-forcing displacement to the end of the base plate on the friction side. Since this is a boundary nonlinear problem with contact conditions, it was solved statically as a sequential analysis with the maximum forced displacement increment set to 1/100 of the maximum forced displacement.

2.4. Method

2.4.1 Hypothesize

The main friction in high-strength bolt joints is friction that propagates instantaneously across single or multiple contact surfaces and generates large relative displacements between steel plates, often resulting in a sudden decrease in the axial stiffness of the joint.

In joints that exhibit a well-defined friction resistance point, the initiation of principal friction causes the axial stiffness of the joint to instantaneously turn negative and the relative displacement between the steel plates to increase rapidly.

Although the mechanism of occurrence of such principal friction is not always clear, this study assumes that it is an unstable phenomenon in which loss of shear stiffness and localized friction occur in a chain model starting from a microscopic region where a certain limit state is first reached on the joint surface (starting point) and propagate to the surrounding area. The main friction is assumed to originate from the region of high frictional shear stress.

This study focuses on whether a limit state for local friction is established at the assumed onset point. Coulomb's law is assumed as the local limit state. Coulomb's law states that the following equation holds for the maximum value of frictional shear stress τ transmitted by a small surface area.

$$Max\ (\tau interface) = \mu pinterface \tag{1}$$

Where μ and $pinterface$ are respectively the static friction coefficient and the contact pressure of the small surface area.

From (1), we can assume $\tau interface\ /\ pinterface$ as the driving parameter for the generation of localized friction. The present study applies a local approach to consider this local trigger introducing two parameters, stress ratio, and Weibull stress ratio, as described later.

2.4.2 Stress Ratio

This study investigates the possibility of estimating the occurrence of local friction based on the stress values evaluated at the integration points of finite elements to investigate a method to evaluate the limit of principal friction occurrence from a simple finite element analysis. The $\tau interface\ /\ pinterface$ (the stress ratio) is defined for a small surface area, which is the ratio of the shear stress τIP to the direct stress σIP evaluated at the integration point of the finite element forming the surface layer.

$$\rho = \tau IP/\sigma IP \tag{2}$$

Eq. (2) focuses on the maximum stress ratio at the onset of friction resistance around the bolt holes of the contact surface and examines whether the maximum stress ratio can be used to evaluate the main friction onset limit state. If the contact surfaces are finished similarly, the friction limit's stress ratios should match. In other words, in the case of the PB specimen, the stress ratio of the friction limit of the single-lap bolt joints should match the stress ratio of the friction limit of the double-lap bolt joints. In the MB specimen, the stress ratio of the friction limit of the 345-rows joints should match the stress ratio of the friction limit of the 2-row joints.

2.4.3 Weibull Stress Ratio

The prediction accuracy of the limit of occurrence of principal friction may be improved by considering local variations in surface properties at the joint surface of a high-strength bolt joint. In this study, the Weibull stress concept, which has been used to evaluate the failure limit of brittle materials [16], is applied to the evaluation of the occurrence limit of principal friction at the joint surface. Weibull stress is formulated based on the weakest link hypothesis, which states that brittle fracture of a material is induced when the basic volume containing defects fails due to equivalent stress in a material-specific probability distribution and that the relationship between generated stress and material failure probability follows a Weibull distribution [17]. In this study, the Weibull stress ratio is

defined as the equivalent stress to the stress ratio for the element in the surface layer as shown in the following equation to apply to the principal friction.

$$\sigma_w = \left(\sum_{i=1}^{n} \rho_i^m S_i\right)^{\frac{1}{m}} \tag{3}$$

Here, n is the number of surface finite elements in the region Ω where high shear stress is generated. The threshold Ω of shear stress is discussed in the next section. ρ And S is the stress ratio of finite elements in the area of the surface. Weibull parameter m gets bigger when the dispersion in each specimen gets smaller. The Weibull stress ratio is higher when the maximum value of the stress ratio is higher and when Ω is wider. Fig. 4 illustrates the Weibull stress ratio concept. The Weibull stress ratio concept models the contact surface as a series of basic surface areas, including defects, and considers that an increase in the stress ratio induces the main friction across the entire contact surface by causing one of the basic surface areas to friction.
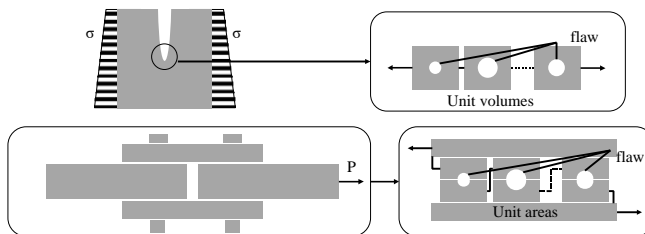

Fig. 4 Concept of Weibull stress ratio

Based on (3), if the contact surfaces are finished in the same way, the Weibull stress ratios at the friction limit should match. In other words, in the case of the PB specimen, the Weibull stress ratio of the friction limit of the single-lap bolt joints should match the Weibull stress ratio of the friction limit of the double-lap bolt joints. In the MB specimen, the Weibull stress ratio of the friction limit of the 345-row joints should match the Weibull stress ratio of the friction limit of the 2-row joints.

3. Results and Discussion

3.1. Calculation Region

The region Ω is mainly determined by the portion of the contact surface in the resolution that is actually in contact. Some of the unstable outermost elements are removed according to the actual situation. The region Ω was calculated for multiple loads and was selected to satisfy the above conditions at any load level, although it was calculated densely around loads equivalent to the friction capacity.

Fig. 5 shows the threshold values for the direct stress σ and the distribution of direct stresses on the joint surface at the friction force. As an example of the blasted specimen, the area Ω determined by the threshold values in the figure generally corresponds to the area of damage on the contact surface after the test, which means the Copen of the element is smaller than 0.

3.2. Varying Numbers of Contracting Surface Prediction by Stress Ration

Fig. 6 shows the relationship between the maximum value of stress ratio ρ and load in the region Ω obtained from the analysis results. Single/double-lap bolt joint specimens are shown separately for each contact surface specification. The maximum stress ratio increases monotonically with load in all specimens, and the location of the point of

maximum stress ratio at the load value equivalent to friction capacity is close to each other among the three specimens of the same type, indicating that the friction capacity and the friction coefficient of the specimens can be estimated from the maximum stress ratio. For the specimens with double-lap bolt joints, it is shown that the prediction of the main friction limit can be obtained.
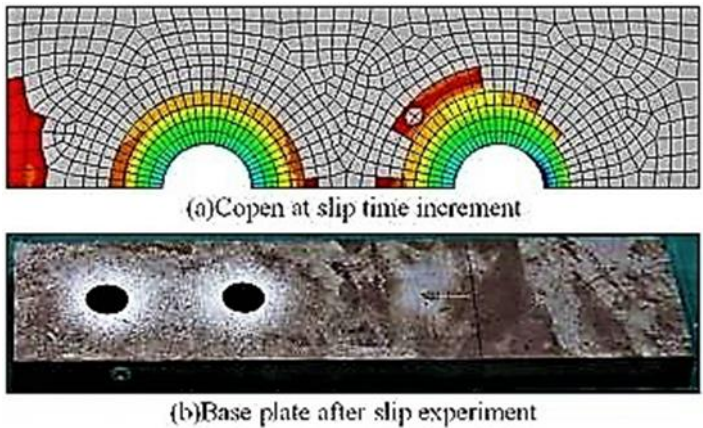

(a)Copen at slip time increment

(b)Base plate after slip experiment

Fig. 5 Result for B2-10-1

(a) IOZ double-lap bolt joints

(b) IOZ single-lap bolt joints

(c) Rust double-lap bolt joints

(d) Rust single-lap bolt joints

Fig. 6 Stress ratio results for different numbers of surfaces

Based on the average of the maximum stress ratios at the friction capacity points for the specimens with double-lap bolt joints, the critical maximum stress ratios for principal friction for the IOZ and blasted specimens were respectively 1.468 and 1.829 for the analysis. According to section 4.2, the friction capacity and coefficient of friction estimated from the maximum stress ratios at the friction capacity points of the double-lap bolt joints

and the identified critical maximum stress ratio of the single-lap bolt joints are shown in Table 3.

Table 3. The prediction result in different numbers of contact surface by using stress rations

Specimens name	The limit value of the stress ratio	Estimated friction Reaction force [kN]	Estimated friction coefficient	Estimation error	Average error
P1-15-1	1.468	124	0.454	-2.87%	6.28%
P1-15-2		132	0.595	12.17%	
P1-15-3		132	0.591	9.84%	
B1-10-1	1.829	133	0.606	-14.90%	-4.82%
B1-10-2		142	0.628	5.00%	
B1-10-3		144	0.635	-4.56%	

Fig. 7 shows the relationship between the Weibull stress ratio ρ and load in the region obtained from the analysis results. Same with the maximum stress ratio, the Weibull stress ratio ρ at a load value equivalent to the friction capacity and the monotonic increase in the Weibull stress ratio ρ with increasing load indicates that the Weibull stress ratio ρ can estimate the friction capacity as well as the friction coefficient. For the specimens with double-lap bolt joints, it is shown that the prediction of the main friction limit can be obtained.

(a) IOZ double-lap bolt joints   (b) IOZ single-lap bolt joints

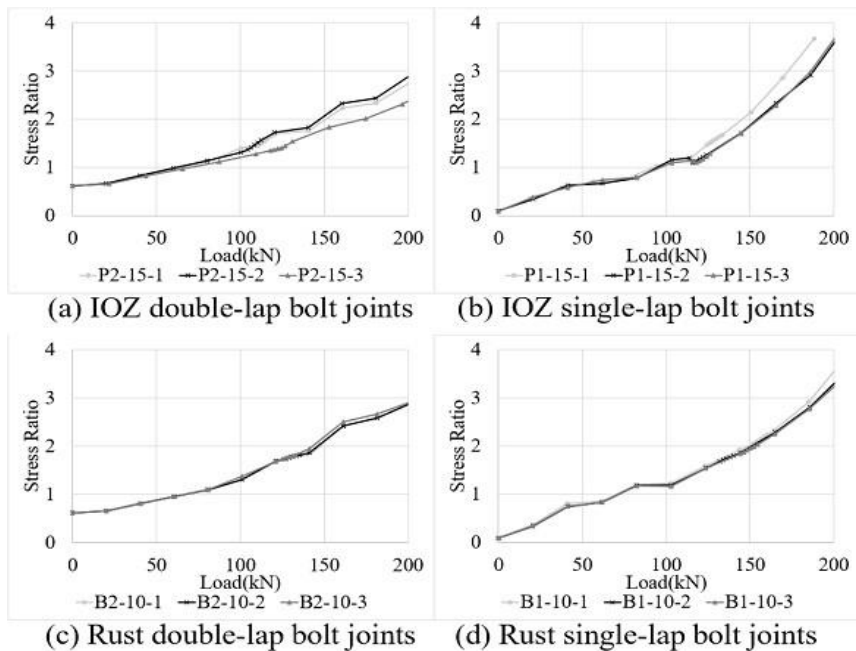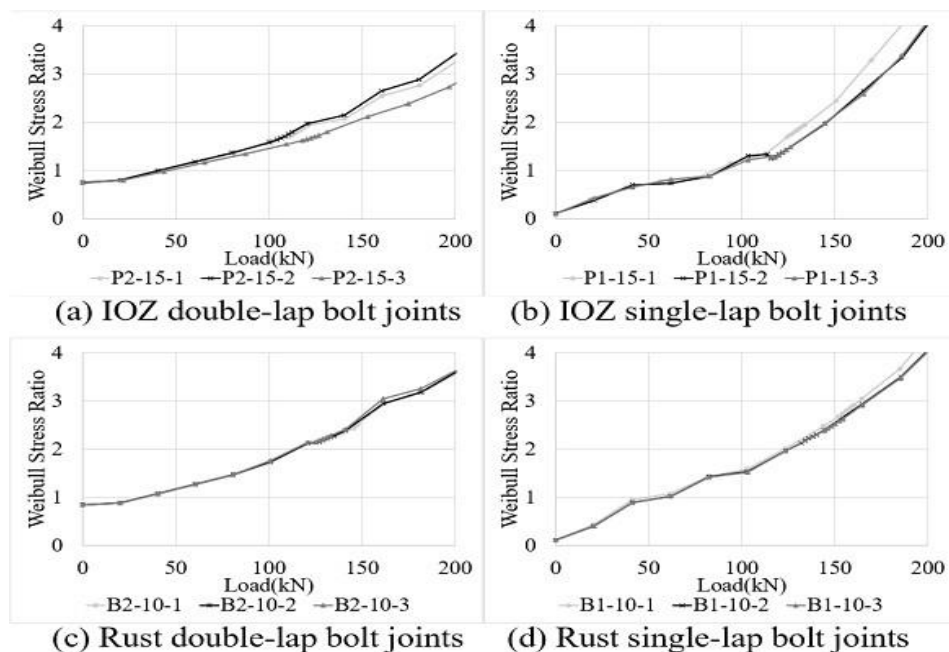(c) Rust double-lap bolt joints   (d) Rust single-lap bolt joints

Fig. 7 Weibull stress ratio results for different numbers of surfaces

Based on the average of the Weibull stress ratios at the friction capacity points for the specimens with double-lap bolt joints, the critical maximum stress ratios for principal friction for the IOZ and blasted specimens were respectively 1.721 and 2.285 for the analysis. According to section 4.2, the friction capacity and coefficient of friction estimated

from the Weibull stress ratios at the friction capacity points of the double-lap bolt joints and the identified critical maximum stress ratio of the single-lap bolt joints are shown in Table 4.

Table 4. The prediction result in different numbers of contact surface by using Weibull mathematical stress rations

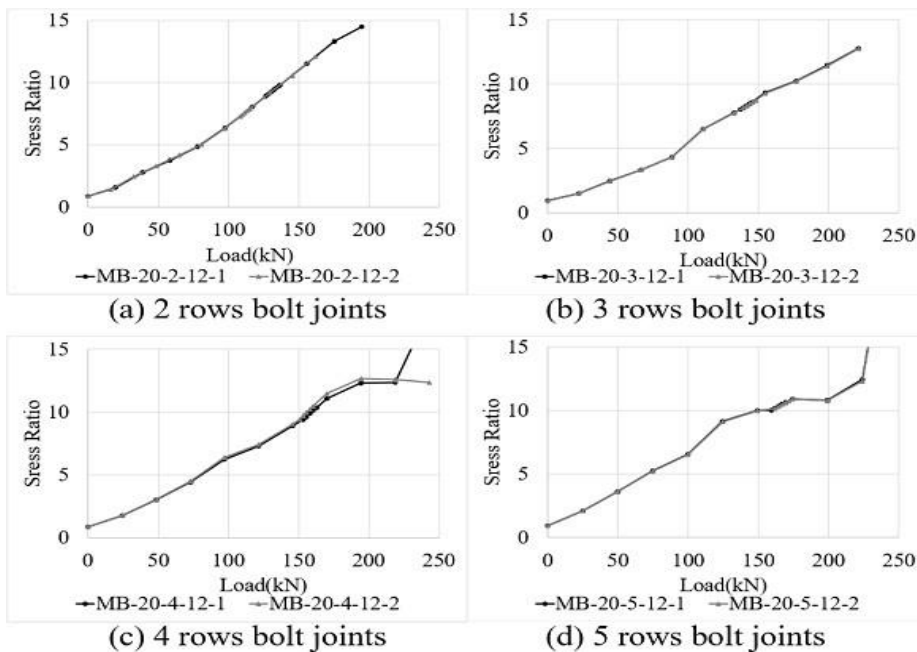| Specimens name	Limit value of Weibull stress ratio	Estimated friction Reaction force [kN]	Estimated friction Coefficient	Estimation error	Average error
P1-15-1		125	0.549	-2.14%	
P1-15-2	1.721	133	0.600	13.05%	6.92%
P1-15-3		132	0.591	9.84%	
B1-10-1		133	0.606	-14.90%	
B1-10-2	2.285	140	0.619	3.48%	-6.24%
B1-10-3		140	0.617	-7.29%	

Fig. 8 Stress ratio results for different numbers of bolts

Fig. 8 shows the relationship between the maximum value of stress ratio ρ and load in the region Ω obtained from the analysis results. Single/double-lap bolt joint specimens are shown separately for each contact surface specification. The maximum stress ratio increases monotonically with load in all specimens, and the location of the point of maximum stress ratio at the load value equivalent to friction capacity is close to each other among the three specimens of the same type, indicating that the friction capacity and the friction coefficient of the specimens can be estimated from the maximum stress ratio. For

the specimens with double-lap bolt joints, it is shown that the prediction of the main friction limit can be obtained.

Based on the average of the maximum stress ratios at the friction capacity points for the specimens with double-lap bolt joints, the critical maximum stress ratios for principal friction for 2 rows of bolt joints specimens is 8.505 for the analysis. According to section 4.2, the friction capacity and coefficient of friction estimated from the maximum stress ratios at the friction capacity points of the 2-rows bolt joints and the identified critical maximum stress ratio of the 3,4,5 rows bolt joints are shown in Table 5.

Table 5. The prediction result in different numbers of bolt rows by using stress rations

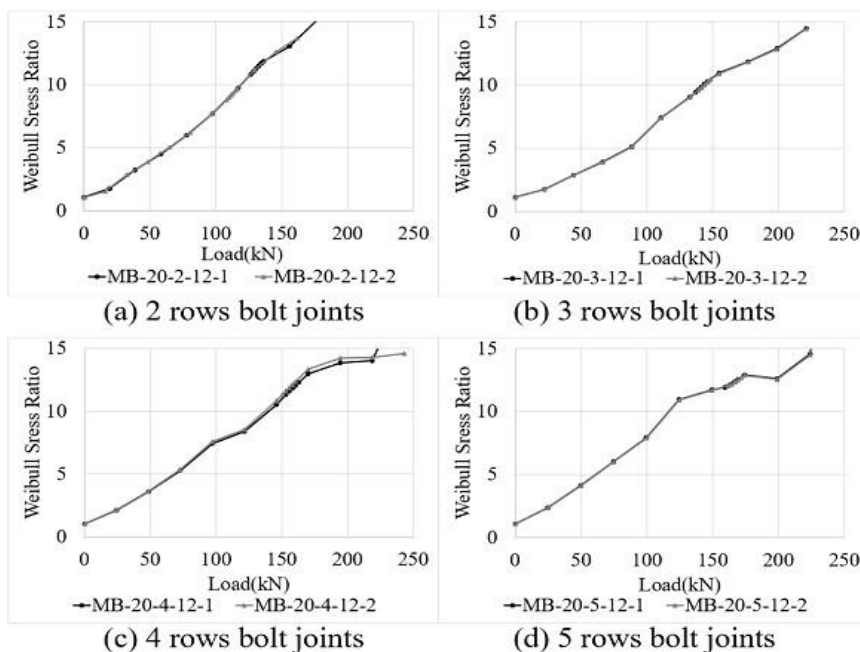| The limit	The limit value of the stress ratio	Estimated friction Reaction force [kN]	Estimated friction coefficient	Estimation error	Average error
MB-20-3-12-1	8.340	576	0.521	0.99%	0.47%
MB-20-3-12-2		576	0.519	-0.04%	
MB-20-4-12-1	9.941	564	0.384	-11.12%	-10.10%
MB-20-4-12-2		564	0.392	-9.08%	
MB-20-5-12-1	10.477	468	0.258	-28.83%	-29.68%
MB-20-5-12-2		468	0.257	-30.54%	

Fig. 9 Weibull stress ratio results for different numbers of bolts

Fig. 9 shows the relationship between the Weibull stress ratio ρ and load in the region obtained from the analysis results. Same with the maximum stress ratio, the Weibull

stress ratio ρ at a load value equivalent to the friction capacity and the monotonic increase in the Weibull stress ratio ρ with increasing load indicates that the Weibull stress ratio ρ can estimate the friction capacity as well as the friction coefficient. For the specimens with double-lap bolt joints, it is shown that the prediction of the main friction limit can be obtained.

Table 6. The prediction results in different numbers of bolt rows by using Weibull mathematical stress rations

Specimens name	Limit value of Weibull stress ratio	Estimated friction Reaction force [kN]	Estimated friction coefficient	Estimation error	Average error
MB-20-3-12-1	9.941	584	0.529	2.39%	2.18%
MB-20-3-12-2		587.6	0.529	1.97%	
MB-20-4-12-1	11.844	573.2	0.390	-9.67%	-9.38%
MB-20-4-12-2		564	0.392	-9.08%	
MB-20-5-12-1	12.351	478	0.264	-27.31%	-28.18%
MB-20-5-12-2		478	0.262	-29.05%	

Based on the average of the Weibull stress ratios at the friction capacity points for the specimens with two-row bolt joints, the critical maximum stress ratio for principal friction is 10.315 for the analysis. According to section 4.2, the friction capacity and coefficient of friction estimated from the Weibull stress ratios at the friction capacity points of the 2 rows of bolt joints and the identified critical maximum stress ratio of the 3, 4, and 5 bolt joints are shown in Table 6.

4. Conclusions

In this research, replacing the friction coefficient, two new parameters, the stress ratio, and the Weibull stress ratio, are introduced to infer the friction limit of bolt joints. For each method, two prediction scenarios were considered: different numbers of contact surfaces and different numbers of bolt columns. Positive results for prediction accuracy were observed. The findings could be summarized as follows.

- For varying numbers of contact surfaces prediction, the slip limit of single-lap bolt joints with IOZ and blasted surface were inferred from those of double-lap bolt joints. The stress and Weibull stress ratios showed a high prediction accuracy.
- For varying numbers of joint rows prediction, the friction limit of 3, 4, and 5 rows of bolt joints with blasted material were inferred from those of 2 rows of bolt joints. Both the stress ratio and the Weibull stress ratio showed higher prediction accuracy than friction coefficients in the prediction of 3-column joints. On the other hand, the accuracy of both the stress ratio and the Weibull stress ratio was low in the 4 and 5 columns joints prediction. It could be considered that the friction/yield ratio is much larger than 1 which means yield happens. Future research is needed to find out explanations for the different results and raise the accuracy by using plastic materials in simulation.

The feasibility of the two new methods was confirmed. They could currently be applied to predict friction limits of bolt joints in different numbers of contact surfaces and joint rows. Their feasibility for other situations will be researched in the future, such as bolt joints with large eccentric or over double-laps.

References

[1] Ministry of Construction of the People's Republic of China. Code for design of steel structures (GB 50017-2003). Beijing. 2003 [in Chinese].

[2] Ministry of Construction of the People's Republic of China. Specification for design, construction, and acceptance of high-strength bolt connections in steel structures (JGJ 82-91). Beijing. 1992 [in Chinese].

[3] Ministry of Railways of the People's Republic of China. Code for design on the steel structure of Railway Bridge (TB10002.2-2005). Beijing. 2005 [in Chinese].

[4] American Institute of Steel Construction. Specification for Structural Steel Buildings. Chicago (IL). 2005.

[5] Kitada T, Yamaguchi T, Matsumura M, et al. New technologies of steel bridges in Japan. Journal of Constructional Steel Research 2002; 58(1):21-7 https://doi.org/10.1016/S0143-974X(01)00029-3

[6] Y. Tamba, S. Yukito, S. Kimura, T. Yamaguchi, K. Sugiura, "Slip coefficient for high strength bolted frictional joints with the roughened steel surface and inorganic Zinc-rich painted surface, Journal of JSCE, A1, Vol. 3, 2015, pp. 19-32. https://doi.org/10.2208/journalofjsce.3.1_19

[7] K. Minami, H. Tamura, N. Yoshioka, D. Uchida, M. Moro, K. Ando, A study on initial bolt pretensions of high strength bolted joints considering a number of contact surfaces. Journal of JSCE, A1, Vol. 75, No.1, 2019, pp. 46-57. https://doi.org/10.2208/jscejseee.75.46

[8] S. Tsujioka, W. Kozo, Strength of M20, and F10T High-Strength Multi bolted slip-Type Joints, Journal of Structural Engineering. B, Vol.40, 1994, pp. 495-500.

[9] Citipitioglu Am H.R.W.D. Refined 3D finite element modeling of partially restrained connections including friction. Journal of Constructional Steel Research2002; 58(8):995-1013. https://doi.org/10.1016/S0143-974X(01)00087-6

[10] Chung KF, Ip KH. Finite element investigation on the structural behavior of cold-formed steel bolted connections. Engineering Structures 2001; 23:1115-25. https://doi.org/10.1016/S0141-0296(01)00006-2

[11] Ju SH, Fan CY, Wu GH. Three-dimensional finite elements of steel bolted connections. Engineering Structures 2004; 26(3):403-13. https://doi.org/10.1016/j.engstruct.2003.11.001

[12] Soo Kim T, Kuwamura H. Finite element modeling of bolted connections in thin-walled stainless steel plates under static shear. Thin-Walled Structures2007; 45(4):407-21. https://doi.org/10.1016/j.tws.2007.03.006

[13] Su RKL, Siu WH. Nonlinear response of bolt groups under in-plane loading. Engineering Structures 2007; 29(4):626-34. https://doi.org/10.1016/j.engstruct.2006.06.003

[14] Yu H, Burgess IW, Davison JB, et al. Numerical simulation of bolted steel connections in fire using explicit dynamic analysis. Journal of Constructional Steel Research 2008; 64(5):515-25. https://doi.org/10.1016/j.jcsr.2007.10.009

[15] Bouchair A, Averseng J, Abidelah A. Analysis of the behavior of stainless steel bolted connections. Journal of Constructional Steel Research 2008; 64(11):1264-74. https://doi.org/10.1016/j.jcsr.2008.07.009

[16] F. Minami, Fracture assessment method using the Weibull stress- Part I, Journal of the Japan Welding Society, Vol.75, No.5, 2005, pp. 416-446. https://doi.org/10.2207/jjws.75.416

[17] C.He, H. Tamura, H. Yamada, H. Katsuchi, Analytical simple estimation of slip coefficient of high strength bolt joints, Journal of Construction Steel, Vol 28, 2020.11, pp. 146-157.